Localized proton magnetic resonance spectroscopy of lipids in adipose tissue at high spatial resolution in mice in vivo

Klaus Strobel,[1],* Joerg van den Hoff,*,† and Jens Pietzsch*

Institute of Radiopharmacy,* Research Center Dresden-Rossendorf, Dresden, Germany; and Department of Nuclear Medicine,† University of Technology, Dresden, Germany

Abstract   We describe a localized proton magnetic resonance spectroscopy (^{1}H-MRS) method for in vivo measurement of lipid composition in very small voxels (1.5 mm × 1.5 mm × 1.5 mm) in adipose tissue in mice. The method uses localized point-resolved spectroscopy to collect ^{1}H spectra from voxels in intra-abdominal white adipose tissue (WAT) and brown adipose tissue (BAT) deposits. Nonlinear least-squares fits of the spectra in the frequency domain allow for accurate calculation of the relative amount of saturated, monounsaturated, and polyunsaturated fatty acids. All spectral data are corrected for spin-spin relaxation. The data show BAT of NMRI mice to be significantly different from BAT of NMRI *nu/nu* mice in all aspects except for the fraction of monounsaturated fatty acids (FM); for WAT, only the FM is different. BAT and WAT of NMRI mice differ in the amount of saturated and diunsaturated fatty acids. This method provides a potential tool for studying lipid metabolism in small animal models of disease during the initiation, progression, and manifestation of obesity-related disorders in vivo.⬛ Our results clearly demonstrate that localized ^{1}H-MRS of adipose tissue in vivo is possible at high spatial resolution with voxel sizes down to 3.4 ml.—Strobel, K., J. van den Hoff, and J. Pietzsch. Localized proton magnetic resonance spectroscopy of lipids in adipose tissue at high spatial resolution in mice in vivo. *J. Lipid Res.* 2008. 49: 473–480.

Supplementary key words   adipocytes • spin-spin relaxation time T_2 • exponential decay • triglyceride • triacylglycerol • nuclear magnetic resonance

Noninvasive in vivo phenotyping of adipose tissue deposits in animal (rodent) models of disease during the initiation, progression, and manifestation of obesity and obesity-related disorders is a need in preclinical metabolic research (1). MRI and [1]H-magnetic resonance spectroscopy (MRS) have been applied recently to provide information on *i*) the distribution of different fat deposits, *ii*) the total amount of fat in these deposits, and *iii*) deposit-specific fat composition in terms of the degree of polyunsaturation of the aliphatic lipid chains in small laboratory animals developing obesity (2–5). Furthermore, the disease-related presence and accumulation of lipids in other organs (e.g., liver, brain, and kidney) or in the skeletal musculature could be evaluated by these techniques in vivo (6–8). There is evidence that in rodent models, both white adipose tissue (WAT) and brown adipose tissue (BAT) are active participants in numerous physiological and pathophysiological processes (1). WAT is the physiological site of energy storage as lipids and for insulation purposes and the provision of a protective cushion. BAT is the primary site of nonshivering thermogenesis during cold acclimatization. The accumulation of excess WAT has been shown to play a crucial role in the development of cardiovascular, metabolic, and renal disorders, including insulin resistance, diabetes mellitus, hyperlipidemia, atherosclerosis, hypertension, and chronic renal disease, many of which are interdependent. On the other hand, BAT in rodents plays a significant role in preventing obesity and insulin resistance.

In this regard, it has become clear that adipose tissue plays an extremely important role as a regulator of the flow of energy-providing substances. Indeed, it stores triacylglycerols but also is an efficient director of nonesterified fatty acids either into adipose tissue for storage or into the circulation as an energy supply for other tissues. Visceral fat, independent of other deposits or their amounts, plays an important role in modulating hepatic insulin action. In this line, adipose tissue distribution, lipid composition, levels of specific lipid oxidation products, and

Abbreviations: AUC, area under the curve; BAT, brown adipose tissue; FD, fraction of diunsaturated fatty acids; FM, fraction of monounsaturated fatty acids; FOV, field of view; FP, fraction of polyunsaturated fatty acids; FS, fraction of saturated fatty acids; FT, fraction of triunsaturated fatty acids; MCL, mean chain length; MRS, magnetic resonance spectroscopy; NEX, number of repetitions; PRESS, point-resolved spectroscopy; TE, echo time; TR, repetition time; WAT, white adipose tissue; WPF, water proton fraction.

[1] To whom correspondence should be addressed.
    e-mail: k.strobel@fzd.de

certain lipid metabolites play crucial roles (9). However, the detailed noninvasive measurement of these parameters in small laboratory animals is a challenge because of the small spatial dimensions of the target structures. Recently, great efforts have been undertaken to minimize the voxel size for spectroscopic measurements in adipose tissue at maximum information content (2–4, 6, 7). To date, voxel sizes down to 3 mm × 3 mm × 3 mm (27 ml) have been realized with localized spectroscopy methods (2), and sizes down to 2.5 mm × 2.5 mm × 6 mm (37.5 ml) have been realized using spectroscopic imaging (chemical shift imaging) techniques (3).

In the present study, we evaluated an improved ^{1}H-MRS method for in vivo measurements of lipid composition in adipose tissue deposits in mice with a voxel size minimized to 1.5 mm × 1.5 mm × 1.5 mm (3.4 ml) by preservation of complete spectral information using a 7 T small animal magnetic resonance tomograph. The method incorporates a correction for spin-spin relaxation. Corrected lipid spectra obtained from such small voxel sizes are a prerequisite for the detailed metabolic characterization and differentiation of small adipose tissue deposits or small regions within larger deposits in rodent models of disease.

MATERIALS AND METHODS

Experimental

Animal experiments are performed using 7–14 week old NMRI female mice (n = 4) and NMRI *nu/nu* female mice (n = 3) according to the guidelines of the German Regulations for Animal Welfare. The protocol (Verification of Prospective Radiopharmaceuticals) is approved by the local Ethical Committee for Animal Experiments. All animals are housed at constant temperature (24°C) with a 12 h light/dark cycle and free access to standard mouse chow and water. The animals are anesthetized with urethane (1.3 g/kg body weight). The animals under anesthesia are then positioned and immobilized prone inside the tomograph with either the thoracic or the abdominal region in the center of the field of view (FOV). After the measurements, animals are euthanized under urethane anesthesia by dislocation of the cervical vertebrae.

Measurements are performed with a 7 T small animal magnetic resonance tomograph with a 30 cm bore (BioSpec® 70/30; Bruker BioSpin MRI GmbH, Ettlingen, Germany) equipped with a mini imaging gradient coil system (gradient strength, 400 mT/m) and a ^{1}H transmit-receive quatrature coil with 72 mm inner diameter. Multislice, respiratory-gated, coronal (FOV = 6 cm × 6 cm, slice thickness = 1.5 mm) and transaxial (FOV = 4 cm × 4 cm, slice thickness = 1.2 mm) spin-echo images are collected with a repetition time (TR) of 480 ms, an echo time (TE) of 14.9 ms, a 256 × 256 data matrix, and a number of repetitions (NEX) of 4.

We use a point-resolved spectroscopy (PRESS) sequence for localized ^{1}H-MRS with TR = 1,800 ms, TE = 20 ms, and NEX = 100–1,000. This sequence uses a combination of magnetic field gradients and frequency-selective 180° pulses to select a three-dimensional voxel of well-defined position and size, whose spectrum is then collected and analyzed. For the measurement of the different adipose tissue deposits in mice, we select voxels of the size from 1.5 mm × 1.5 mm × 1.5 mm to 3 mm × 3 mm × 3 mm depending on the sizes of the fat deposit (**Figs. 1**, **2**).
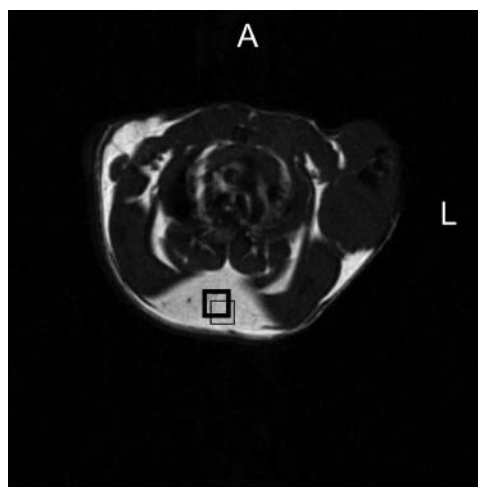

Fig. 1. Transaxial MRI slice through the neck region where the brown adipose tissue (BAT) is located. We use a spin-echo sequence with repetition time (TR) = 480 ms, echo time (TE) = 14.9 ms, field of view (FOV) = 4 cm × 4 cm, slice thickness = 1.2 mm, 256 × 256 data matrix, and number of repetitions (NEX) = 4. The voxel position used to measure the BAT proton spectra is indicated by the thick black square. Also shown is the chemical shift displacement of the fat peak at 1.3 ppm (thin black square) to illustrate the fat-water shift of the point-resolved spectroscopy (PRESS) sequence used. The positioning of the mouse is indicated by the letters A (anterior) and L (left).

A gradient strength up to 160 mT/m is used to achieve such small voxel sizes. Figures 1 and 2 also show the chemical shift displacement of the voxels between the water peak (thick black squares) and the lipid peak at 1.3 ppm (thin black squares) (**Fig. 3**, **Table 1**). The spatial displacement ranges from 19% to
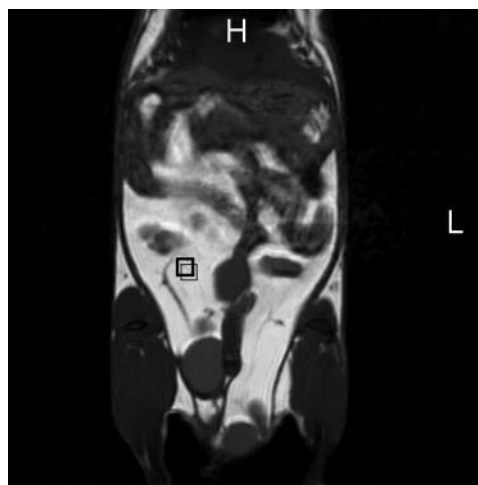
Fig. 2. Coronal MRI slice through the abdominal region where the intra-abdominal white adipose tissue (WAT) is located. We use a spin-echo sequence with TR = 480 ms, TE = 14.9 ms, FOV = 6 cm × 6 cm, slice thickness = 1.5 mm, 256 × 256 data matrix, and NEX = 4. The voxel position used to measure the intra-abdominal WAT proton spectra is indicated by the thick black square. Also shown is the chemical shift displacement of the fat peak at 1.3 ppm (thin black square) to illustrate the fat-water shift of the PRESS sequence used. The positioning of the mouse is indicated by the letters H (head) and L (left).
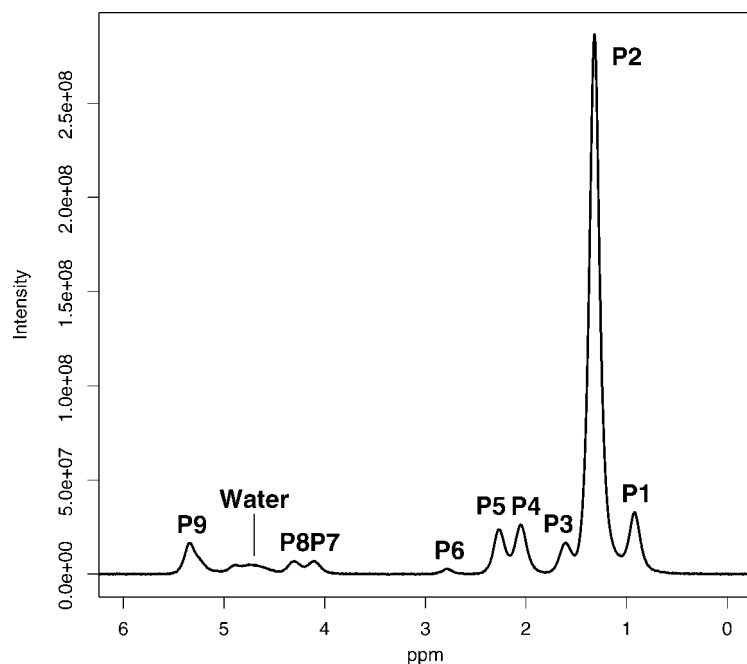
Fig. 3. Representative localized in vivo proton spectrum (PRESS: TR = 1.8 s, TE = 20 ms, voxel size = 2 mm × 2 mm × 2 mm, NEX = 500) of adipose tissue of a mouse. Shown are nine different lipid peaks (P1 at 0.90 ppm, P2 at 1.30 ppm, P3 at 1.60 ppm, P4 at 2.03 ppm, P5 at 2.25 ppm, P6 at 2.76 ppm, P7 at 4.09 ppm, P8 at 4.28 ppm, and P9 at 5.32 ppm) characteristic of a spectrum of triacylglycerol and the resonance peak of water at 4.7 ppm.

30% of the voxel sizes used in the PRESS sequence. Before measurement, the automatic shimming procedure FASTMAP (10) is used to achieve optimal uniformity of the magnetic field across the voxel volume. We use no water suppression in all PRESS sequences during measurement. The free induction decay signals are Fourier-transformed, and the phase and the baseline of the spectra are corrected using TOPSPIN (Bruker BioSpin MRI GmbH). The phase and baseline corrections have to be performed with great care, because the results are very sensitive to mismatches regarding these corrections. No line-broadening is applied to the spectral data.

Calibration of MRS data, calculation of lipid composition, and statistical analysis

In Table 1, the nine peak positions of the different peaks (Fig. 3) are shown, which correlate with the different positions of the ^{1}H in triacylglycerols. The contribution of nonesterified fatty acids to the measured signal is negligible, because the amount of them is very small (11). We use a localized PRESS sequence with a TR of 1.8 s and a series of different TEs to calculate the different spin-spin relaxation times (T_2) of the single

TABLE 1. Correspondence of nine different peaks (P_1–P_9) in proton magnetic resonance spectra obtained from adipose tissue deposits (Fig. 3) to different ^{1}H positions in triacylglycerols (19)

Peak	Chemical Shift	Triacylglycerol-Associated ^{1}H of the Spectra
P_1	0.90 ppm	C$\underline{H}_3$–(CH$_2$)$_n$–
P_2	1.30 ppm	–(C$\underline{H}_2$)$_n$–
P_3	1.60 ppm	–CH$_2$–O–CO–CH$_2$–C$\underline{H}_2$–
P_4	2.03 ppm	–CH$_2$–C$\underline{H}_2$–CH=CH–
P_5	2.25 ppm	–CH$_2$–O–CO –C$\underline{H}_2$–CH$_2$–
P_6	2.76 ppm	–CH=CH–C$\underline{H}_2$–CH=CH–
P_7	4.09 ppm	–C$\underline{H}_2$–O–C(O)–CH$_2$–CH$_2$–
P_8	4.28 ppm	–C$\underline{H}_2$–O–C(O)–CH$_2$–CH$_2$–
P_9	5.32 ppm	–C$\underline{H}$=C$\underline{H}$– and >C$\underline{H}$–CH$_2$–O–C(O)–CH$_2$–CH$_2$–

The protons responsible for the different signals are shown bold-face and underlined. All spectra are shifted, so that peak 2 is located at 1.30 ppm.

peaks inside a voxel of the abdominal region of the mice, NEX = 64, voxel size = 3 mm × 3 mm × 3 mm. The values of TE range from 12 to 50 ms, with fixed TE1 = 5.25 ms. All measurements are repeated five times for all TE values, including the shimming procedure with FASTMAP before each scan series. We determine T_2 for nine different peaks (in the range from 0.9 to 5.32 ppm) by fitting the monoexponential model function $M_{TE} = M_0 \times \exp(-TE/T_2)$ to the measured peak integrals at the different TEs. Peak P3 is fitted from 12 to 20 ms, because the peak is not separable from the signal of peak P2 for TE > 20 ms. Peaks P7 and P8 are also fitted from 12 to 20 ms, because they are not separable from the signal of the water peak for TE > 20 ms.

The water protons are not fully relaxed in our PRESS sequence, TR = 1.8 s, because the T_1 relaxation time of water protons is nearly equal to TR. To correct the areas under the curves (AUCs) of the proton peaks for T_1 relaxation, we also measured one spectrum in the fully relaxed state using TR = 10 s and one spectrum with TR = 1.8 s. From the difference between the two spectra, we get a correction factor of 1.29 for the water peak. The AUCs of the water protons are multiplied by this factor. The lipid peaks need no correction for T_1 relaxation, because the T_1 relaxation times are much shorter than TR (7).

The AUCs are determined by nonlinear least-squares fitting of appropriate model functions (Gaussian and Lorentz curves). The fitting procedures are implemented using the R programming language (12). The regions from 0 to 3.5 ppm and from 3.5 to 6.0 ppm of the spectra are fitted separately. We use five to seven fitting curves for each region in the fitting algorithm.

From the AUCs (AUC$_1$–AUC$_9$) of the nine lipid peaks (P$_1$–P$_9$) and the AUC of the water proton peak (AUC$_W$), the following properties of triacylglycerols are calculated. The fraction of unsaturated fatty acids is calculated as follows: dividing $1/4 \times AUC_4$ (four protons are involved per fatty acid, producing the signal of P$_4$; see Table 1) by $1/2 \times AUC_5$ (two protons are involved per fatty acid, producing the signal of P$_5$):

$$FU = \frac{1}{2}\frac{AUC_4}{AUC_5} \qquad (Eq.\ 1)$$

Localized MRS of lipids in adipose tissue in mice 475

TABLE 2. Spin-spin relaxation times (T_2) and correction factors (M_0/M_{TE}) for the nine different proton resonances for triacylglycerols and the proton resonance of the water peak

Peak	T_2	M_0/M_{TE} (TE = 20 ms)
	ms	
P_1 = 0.90 ppm	41.66 ± 1.97	1.62 ± 0.04
P_2 = 1.30 ppm	51.43 ± 0.67	1.48 ± 0.01
P_3 = 1.60 ppm	18.95 ± 4.00	2.87 ± 0.48
P_4 = 2.03 ppm	25.74 ± 1.10	2.17 ± 0.06
P_5 = 2.25 ppm	33.49 ± 1.92	1.82 ± 0.06
P_6 = 2.76 ppm	46.96 ± 1.45	1.53 ± 0.02
P_7 = 4.09 ppm	19.47 ± 3.75	2.79 ± 0.42
P_8 = 4.28 ppm	20.47 ± 5.35	2.66 ± 0.49
P_9 = 5.32 ppm	36.44 ± 1.80	1.73 ± 0.04
Water peak = 4.70 ppm	18.14 ± 1.08	3.01 ± 0.18

TE, echo time. The values shown are means ± SD and are valid for the point-resolved spectroscopy sequence used.

The fraction of saturated fatty acids (FS) is:

$$FS = 1 - FU \qquad (Eq.\ 2)$$

The fraction of diunsaturated fatty acids (FD) is:

$$FD = \frac{AUC_6}{AUC_5} - 2FT \qquad (Eq.\ 3)$$

The fraction of triunsaturated fatty acids (FT) can be fixed to see the effect on the fraction of monounsaturated fatty acids (FM) and diunsaturated fatty acids. For FT = 0 in equation 3, one gets FD = FP (where FP is the fraction of polyunsaturated fatty acids). We assume that higher unsaturated fatty acids are scarce in rodent adipose tissue (13) when fed with standard food; therefore, they are neglected in our calculation.

The FM is:

$$FM = FU - FD - FT \qquad (Eq.4)$$

Counting the hydrogen atoms associated with the different carbon atoms and using equations 1 and 4, the mean chain length (MCL) can be written as:

$$MCL = \frac{\frac{1}{3}AUC_1 + \frac{1}{2}AUC_2 \times \left(FS + \frac{28}{20}FM + \frac{28}{14}FD + \frac{28}{8}FT\right) + \frac{1}{2}AUC_3 + \frac{1}{2}AUC_5}{\frac{1}{2}AUC_5} + 1$$

$$(Eq.\ 5)$$

For simplicity, it is assumed that the saturated fatty acids all have a chain length of 16 and the monounsaturated fatty acids, the diunsaturated fatty acids, and the triunsaturated fatty acids all have chain lengths of 18 (13), because all other fatty acids are rare and therefore will change the value of the MCL only slightly. The factors in front of FM, FD, and FT arise from the fact that, in monounsaturated fatty acids, only 20 hydrogen atoms (bound to 10 carbon atoms) are involved in the signal generation of peak P_2. Because peaks P_4 and P_9 (**Table 2**) are not used to calculate the MCL, four carbon atoms are missing in the case of monounsaturated fatty acids. To compensate for this, FM in equation 5 is multiplied by a factor of 28/20. The factors for FD and FT are calculated accordingly.

The water proton fraction (WPF) is defined as:

$$WPF = \frac{AUC_W}{AUC_1 + AUC_2 + AUC_3 + AUC_4 + AUC_5 + AUC_6 + AUC_7 + AUC_8 + AUC_9 + AUC_W}$$

$$(Eq.\ 6)$$

AUC_9 is the sum of the signals of two different resonances (see peak P_9 in Table 1). AUC_9 is used only to calculate the WPF, where the relative magnitude of the signal arising from the glycerol proton (at C_2) is <1% of the value of the WPF. Therefore, WPF is not corrected for this. The relative magnitude of the signal arising from the glycerol proton (at C_2) in peak P_9 alone lies between 15% and 25%.

The statistical significance of differences between corrected and not corrected values, between NMRI and NMRI *nu/nu* mice, and between BAT and WAT is assessed using the nonparametric Mann-Whitney U-test. The Mann-Whitney U-test can
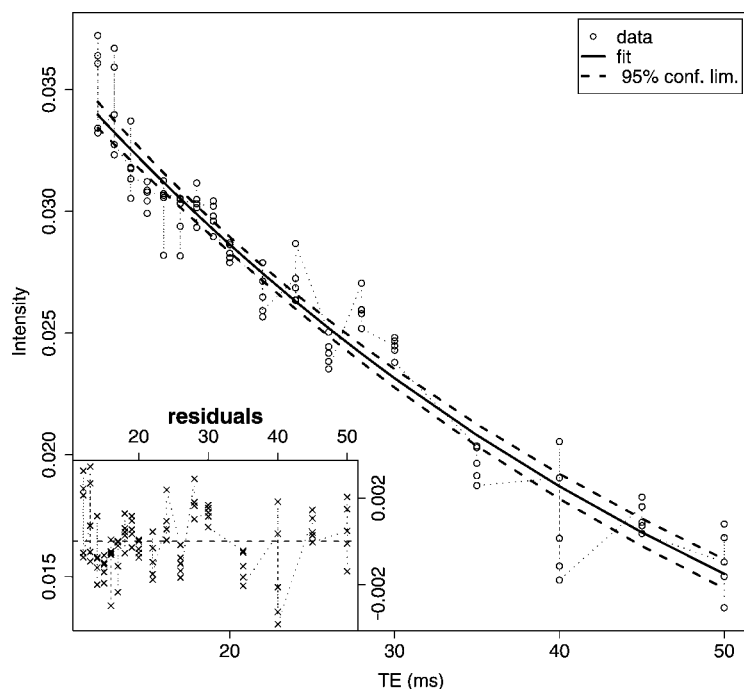

Fig. 4. Example of the T_2 spin-spin relaxation decay of peak 6 at 2.76 ppm. We use a localized PRESS sequence with TR = 1.8 s and a series of different TEs to calculate the different T_2 values inside the abdominal region of a NMRI mouse (NEX = 64, voxel size = 3 mm × 3 mm × 3 mm). The values of TE range from 12 to 50 ms, with fixed TE1 = 5.25 ms. All measurements are repeated five times for all TEs. T_2 is derived by fitting the monoexponential model function $M_{TE} = M_0 \times \exp(-TE/T_2)$ to the measured signal intensities at the different TEs. Shown are the measured data points, the fitting curve, the 95% confidence limits, and the residuals.

be used to calculate P values for the significance of differences within groups of $n_1 = n_2 = 4$ and $n_1 = 3$ versus $n_2 = 4$ but not for $n_1 = n_2 = 3$. In all cases, the criterion of significance is $P < 0.05$.

RESULTS

The derived T_2 relaxation times and the correction factors M_0/M_{TE} for TE = 20 ms for the PRESS sequence applied are summarized in Table 2. The T_2 relaxation times for the nine different proton resonances of triacylglycerols range from 18.95 ± 4.00 ms to 51.43 ± 0.67 ms. The measured T_2 relaxation times are slightly shorter than the true T_2 relaxation times, because the PRESS sequence does not prevent the effects of diffusion and J-coupling (14, 15). These T_2 values lead to correction factors M_0/M_{TE} for the integrals of the peaks ranging from 2.87 ± 0.48 to 1.48 ± 0.01 for a PRESS sequence

with TE = 20 ms. The T_2 relaxation time for the water peak was calculated to be 18.14 ± 1.08 ms, which results in a correction factor of 3.01 ± 0.18 for a PRESS sequence with TE = 20 ms. **Figure 4** exemplarily shows the measured data for peak 6 with the fitted curve, the 95% confidence interval, and the residuals. **Figures 5** and **6** show, as an example, two parts of one localized in vivo spectrum (PRESS: TR = 1.8 s, TE = 20 ms, voxel size = 1.5 mm × 1.5 mm × 1.5 mm, NEX = 1,000) of BAT of a NMRI *nu/nu* mouse, including the fitting curves and the residuals of the fit compared with the measured points. It can be seen that the nine different lipid peaks are clearly distinguishable. The small residuals show that our model curves fit the measured data very accurately. Because of the high spatial resolution in our localized in vivo spectra, it is possible to calculate different properties of the lipids in BAT and WAT, like the fractions of saturated fatty acids, monounsaturated fatty acids, diunsaturated fatty acids (or
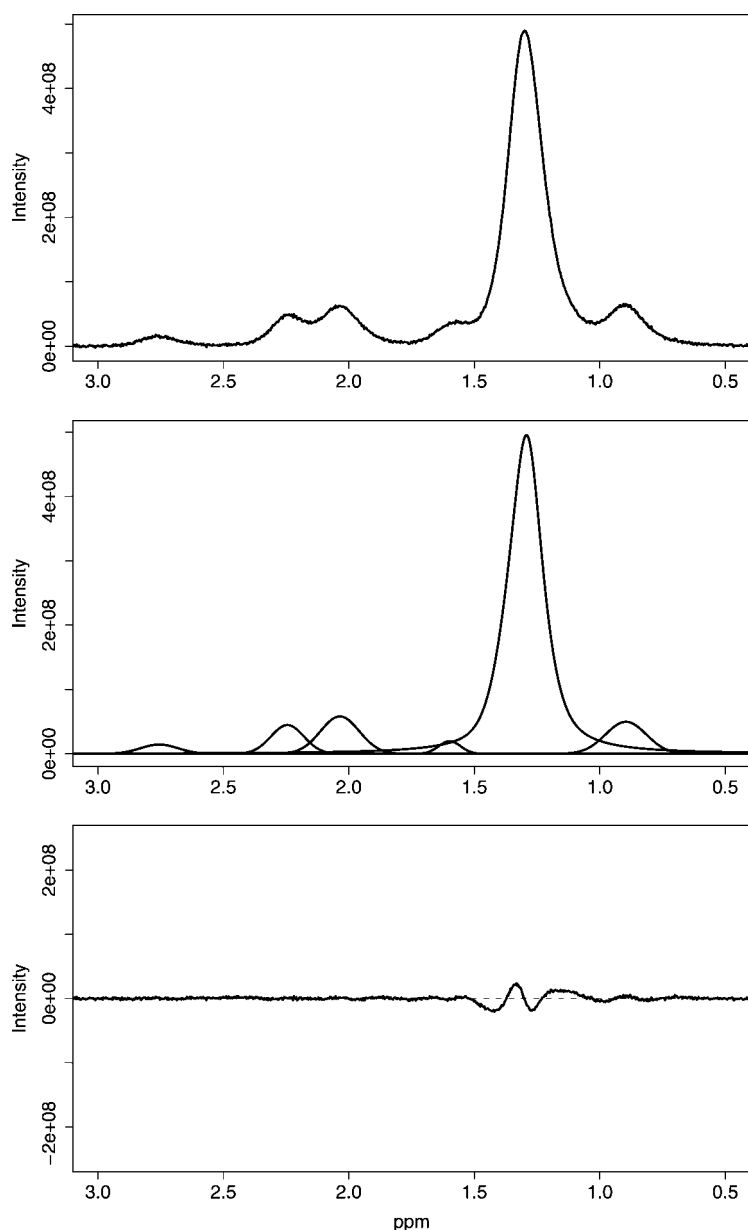
Fig. 5. Localized in vivo proton spectrum (PRESS: TR = 1.8 s, TE = 20 ms, voxel size = 1.5 mm × 1.5 mm × 1.5 mm, NEX = 1,000) obtained from BAT of one NMRI *nu/nu* mouse. Shown is the region between 0.5 and 3.0 ppm. Top: The measured magnetic resonance spectrum. Middle: The single fitting curves for each peak of the fitted spectrum. Bottom: Difference between the measured spectrum and the fitting curves.
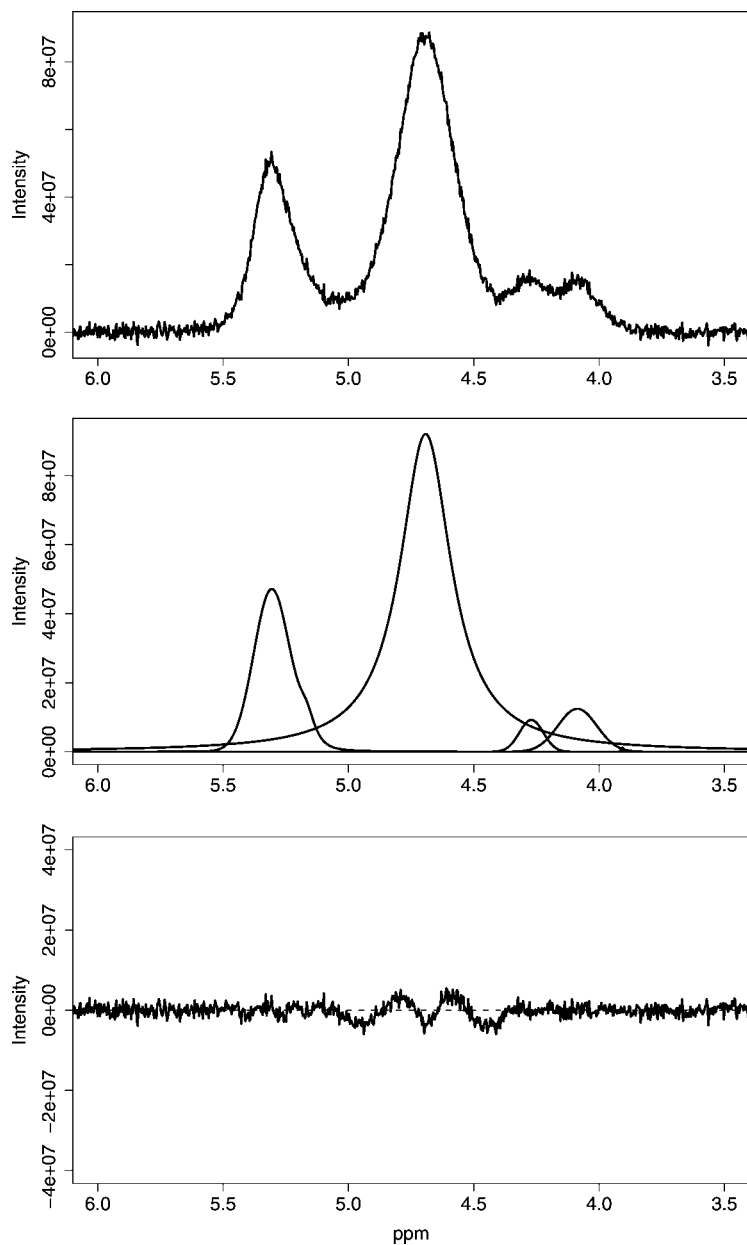
Fig. 6. Localized in vivo proton spectrum (PRESS: TR = 1.8 s, TE = 20 ms, voxel size = 1.5 mm × 1.5 mm × 1.5 mm, NEX = 1,000) obtained from BAT of one NMRI *nu/nu* mouse. Shown is the region between 3.5 and 6.0 ppm. Top: The measured magnetic resonance spectrum. Middle: The single fitting curves for each peak of the fitted spectrum. Bottom: Difference between the measured spectrum and the fitting curves.

polyunsaturated fatty acids, in the case that FT in equation 3 is defined as zero), the MCL, and the WPF. The obtained spectral resolution can be considered as high for in vivo MRS.

Table 3 shows the derived values for the composition of triacylglycerols in the two mouse models (NMRI and NMRI *nu/nu*) for BAT and WAT. Shown are the mean results for each mouse model. For NMRI mice, the differences between the corrected and not corrected results are significant for saturated and monounsaturated fatty acids as well as for the MCL. The corrected and not corrected values of the WPF of BAT in NMRI mice are also significantly different. The measured mean percentage of saturated, monounsaturated, and diunsaturated fatty acids in mice are comparable to values found in the literature (16–18).

Because the relaxation times T_2 are in the range of the TE of the sequence, the localized PRESS spectra of adipose tissue have to be corrected for spin-spin relaxation. Otherwise, the calculated values of the fraction of the different fatty acids are erroneous: deviations from the correct individual/mean values get up to a factor of 3.0/2.2 for saturated fatty acids, a factor of 1.3/1.5 for monounsaturated fatty acids, a factor of 1.4/1.3 for diunsaturated fatty acids, a factor of 1.2 /1.2 for the MCL, and a factor of 1.9/1.8 for the WPF for the animals used in this study. This outcome is also relevant for other localized ^{1}H-MRS methods, like the stimulated echo acquisition mode, or nonlocalized techniques, like spectroscopic imaging, if TE is of the order of T_2 of lipids.

Furthermore, differences between NMRI and NMRI *nu/nu* mice and between BAT and WAT of each mouse

TABLE 3. FS, FM, FD, MCL, and WPF in WAT and BAT of four NMRI mice and three NMRI *nu/nu* mice

Mice	FS	FM	FD	FT Fixed	MCL	WPF
	(UFP; %)			%	(UFP)	(UFP; %)
BAT, NMRI mice						
Corrected	32.6 ± 5.0 (1.5)	59.4 ± 7.0 (1.5)	6.0 ± 2.0 (0.2)	2	17.8 ± 0.7 (0.4)	10.1 ± 1.7 (0.2)
Not corrected	43.5 ± 4.2	46.6 ± 6.6	7.9 ± 2.4	2	20.7 ± 0.6	5.7 ± 1.0
P	<0.05	<0.05	NS		<0.03	<0.03
BAT, NMRI *nu/nu* mice						
Corrected	15.0 ± 6.1 (2.1)	59.2 ± 2.8 (2.2)	23.9 ± 4.8 (0.6)	2	20.4 ± 1.0 (0.6)	25.5 ± 11.7 (0.4)
Not corrected	28.7 ± 5.1	40.2 ± 2.5	29.2 ± 5.7	2	24.0 ± 1.2	16.0 ± 7.9
P	–	–	–		–	–
WAT, NMRI mice						
Corrected	11.8 ± 3.6 (1.9)	62.8 ± 2.2 (2.0)	23.4 ± 3.3 (0.5)	2	18.5 ± 0.5 (0.5)	8.0 ± 7.2 (0.3)
Not corrected	26.1 ± 3.0	43.4 ± 2.4	28.6 ± 1.5	2	21.4 ± 0.6	4.7 ± 4.4
P	<0.05	<0.05	NS		<0.03	NS
WAT, NMRI *nu/nu* mice						
Corrected	12.9 ± 1.0 (2.2)	57.0 ± 1.0 (2.3)	28.2 ± 1.6 (0.7)	2	18.8 ± 0.6 (0.5)	9.2 ± 1.1 (0.2)
Not corrected	26.9 ± 0.8	36.8 ± 1.3	34.3 ± 1.9	2	21.9 ± 0.7	5.3 ± 0.7
P	–	–	–		–	–

BAT, brown adipose tissue; FD, fraction of diunsaturated fatty acids; FM, fraction of monounsaturated fatty acids; FS, fraction of saturated fatty acids; FT, fraction of triunsaturated fatty acids; MCL, mean chain length; UFP, uncertainty resulting from the fitting procedure; WAT, white adipose tissue; WPF, water proton fraction. The FT is fixed to a value of 2%, which is typical for rodent adipose tissue, in which higher unsaturated fatty acids are scarce (13). Shown are the results, corrected for T_2 relaxation, the uncorrected results, and the significance (Mann-Whitney U-test) of differences between the results. If no P value is given, the Mann-Whitney U-test was not applicable.

type are calculated (**Table 4**). We found that BAT of NMRI mice is significantly different from BAT of NMRI *nu/nu* mice in all aspects except for the FM, whereas for WAT, only the FM is different. BAT and WAT of NMRI mice differ significantly in the amount of saturated and diunsaturated fatty acids. For NMRI *nu/nu* mice, no reasonable P value could be calculated because of the small number (n = 3) of animals.

DISCUSSION

We have demonstrated that in vivo ^{1}H-MRS of adipose tissue in rodents at high magnetic field strength (7 T) allows for localized spectroscopy in very small voxels, down to voxel sizes of 1.5 mm × 1.5 mm × 1.5 mm. Because of the fact that the different ^{1}H signals from triacylglycerols

TABLE 4. Significance of differences between BAT and WAT of NMRI and NMRI *nu/nu* mice and between BAT and WAT within the same mouse model

Sample	FS	FM	FD	MCL	WPF
BAT, NMRI mice versus BAT, NMRI *nu/nu* mice					
P corrected	<0.05	NS	<0.05	<0.05	<0.05
P not corrected	<0.05	NS	<0.05	<0.05	<0.05
WAT, NMRI mice versus WAT, NMRI *nu/nu* mice					
P corrected	NS	<0.05	NS	NS	NS
P not corrected	NS	<0.05	NS	NS	NS
BAT, NMRI mice versus WAT, NMRI mice					
P corrected	<0.03	NS	<0.03	NS	NS
P not corrected	<0.03	NS	<0.03	NS	NS
BAT, NMRI *nu/nu* mice versus WAT, NMRI *nu/nu* mice					
P corrected	–	–	–	–	–
P not corrected	–	–	–	–	–

Shown is the significance of differences for the FS, FM, FD, MCL, and WPF. If no P value is given, the Mann-Whitney U-test was not applicable.

have different spin-spin relaxation times (T_2), all spectral data have to be corrected for T_2 relaxation. Otherwise, the content of saturated fatty acids, diunsaturated fatty acids, and the MCL will be overestimated and the content of monounsaturated fatty acids and the WPF will be underestimated (Table 3). Not correcting the spectral data of localized ^{1}H-MRS of adipose tissue for spin-spin relaxation will lead to erroneous values for the fractions of different fatty acids, deviations reaching a factor of 3 in the case of saturated fatty acids.

Other pitfalls that might occur within in vivo localized MRS are *i*) chemical shift displacement, *ii*) spin-spin relaxation, and *iii*) error propagation. Depending on the bandwidth of the excitation pulses and the gradient strength used during excitation, the opposite parts of localized PRESS spectra can be far away in spatial position. As shown in Figs. 1, 2, the chemical shift displacement of the water peak and the lipid peak P_2 at 1.3 ppm are in the range from 19% to 30% of the voxel size. These small displacements are achieved using gradient strength up to 160 mT/m in the PRESS sequence used. Although the chemical shift displacement in the present study is small, the opposite sides of one spectrum are not measured exactly at the same position. One has to keep in mind the fact that the chemical shift displacement is a potential source of error. Furthermore, different ^{1}H signals from triacylglycerols have different spin-spin relaxation times (T_2). Therefore, all spectral data have to be corrected for T_2 relaxation, but this point often receives no adequate consideration. In addition, small errors in the calculated integrals of the individual resonances (e.g., from inadequate baseline correction) can add up to major errors in the calculated fractions of the different fatty acids as a result of error propagation.

In conclusion, the current approach allows the determination of lipid composition by localized ^{1}H-MRS in

adipose tissue deposits in small laboratory animals in vivo. Using this methodology, corrected lipid spectra can be obtained from voxels with a dimension of 1.5 mm $\times$ 1.5 mm $\times$ 1.5 mm, thus providing a potential tool for the characterization and differentiation of small adipose tissue deposits or small regions within larger deposits in rodent models of disease.

REFERENCES

1. Summers, L. K. 2006. Adipose tissue metabolism, diabetes and vascular disease—lessons from in vivo studies. *Diabetes Vasc. Dis. Res.* **3:** 12–21.
2. Calderan, L., P. Marzola, E. Nicolato, P. F. Fabene, C. Milanese, P. Bernardi, A. Giordano, S. Cinti, and A. Sbarbati. 2006. In vivo phenotyping of the *ob/ob* mouse by magnetic resonance imaging and ¹H-magnetic resonance spectroscopy. *Obesity.* **14:** 405–415.
3. Lunati, E., P. Farace, E. Nicolato, C. Righetti, P. Marzola, A. Sbarbati, and F. Osculati. 2001. Polyunsaturated fatty acids mapping by ¹H MR-chemical shift imaging. *Magn. Reson. Med.* **46:** 879–883.
4. Walling, B. E., J. Munasinghe, D. Berrigan, M. Bailey, and R. M. Simpson. 2007. Intra-abdominal fat burden discriminated in vivo using proton magnetic resonance spectroscopy. *Obesity.* **15:** 69–77.
5. Garcia, M. C., I. Wernstedt, A. Berndtsson, M. Enge, M. Bell, O. Hultgren, M. Horn, B. Ahren, S. Enerback, C. Ohlsson, et al. 2006. Mature-onset obesity in interleukin-1 receptor I knockout mice. *Diabetes.* **55:** 1205–1213.
6. Garbow, J. R., X. Lin, N. Sakata, Z. Chen, D. Koh, and G. Schonfeld. 2004. In vivo MRS measurement of liver lipid levels in mice. *J. Lipid Res.* **45:** 1364–1371.
7. Brix, G., S. Heiland, M. E. Bellemann, T. Koch, and W. J. Lorenz. 1993. MR imaging of fat-containing tissues: valuation of two quantitative imaging techniques in comparison with localized proton spectroscopy. *Magn. Reson. Imaging.* **11:** 977–991.
8. Schick, F., B. Eismann, W. I. Jung, H. Bongers, M. Bunse, and O. Lutz. 1993. Comparison of localized proton NMR signals of skeletal muscle and fat tissue in vivo: two lipid compartments in muscle tissue. *Magn. Reson. Med.* **29:** 158–167.
9. Shoelson, S. E., L. Herrero, and A. Naaz. 2007. Obesity, inflammation, and insulin resistance. *Gastroenterology.* **132:** 2169–2180.
10. Gruetter, R. 1993. Automatic, localized in vivo adjustment of all first- and second-order shim coils. *Magn. Reson. Med.* **29:** 804–811.
11. Angel, A., K. S. Desai, and M. L. Halperin. 1971. Intracellular accumulation of free fatty acids in isolated white adipose cells. *J. Lipid Res.* **12:** 104–111.
12. R Development Core Team. 2007. R: A Language and Environment for Statistical Computing. R Foundation for Statistical Computing, Vienna.
13. Raclot, T., and R. Groscolas. 1995. Selective mobilization of adipose tissue fatty acids during energy depletion in the rat. *J. Lipid Res.* **36:** 2164–2173.
14. de Graaf, R. A. 1998. In Vivo NMR Spectroscopy. John Wiley & Sons, Ltd., Chichester, UK.
15. Hennig, J., T. Thiel, and O. Speck. 1997. Improved sensitivity to overlapping multiplet signals in *in vivo* proton spectroscopy using a multiecho volume selective (CPRESS) experiment. *Magn. Reson. Med.* **37:** 816–820.
16. Tove, S. B., and F. H. Smith. 1960. Changes in the fatty acid composition of the depot fat of mice induced by feeding oleate and linoleate. *J. Nutr.* **71:** 264–272.
17. Mohrhauer, H., and R. T. Holman. 1963. The effect of dietary essential fatty acids upon composition of polyunsaturated fatty acids in depot fat and erythrocytes of the rat. *J. Lipid Res.* **4:** 346–350.
18. Hargrave, K. M., B. J. Meyer, C. Li, M. J. Azain, C. A. Baile, and J. L. Miner. 2004. Influence of dietary conjugated linoleic acid and fat source on body fat and apoptosis in mice. *Obes. Res.* **12:** 1435–1444.
19. Lie Ken Jie, M. S. F., and C. C. Lam. 1995. ¹H-nuclear magnetic resonance spectroscopic studies of saturated, acetylenic and ethylenic triacylglycerols. *Chem. Phys. Lipids.* **77:** 155–171.